Searching for the Terrestrial Paleocene/Eocene Boundary at the Canadian High Arctic: A Carbon Isotope Study

The Honors Program
Senior Capstone Project
Monica Kraus
Faculty Advisors: Hong Yang, Brian Blais
Collaborators: Ben A. LePage (The Academy of Natural Sciences and URS Corporation, PA), Mark Pagani (Yale University)
April, 2007

Table of Contents

ABSTRACT

The Paleocene Eocene Thermal Maximum (PETM) is a rare climatic event in the history of the Earth, which marks the abrupt transition from the Paleocene to Eocene of the Cenozoic era with a rapid increase in global surface temperatures of up to 5-8̃C. The PETM marks the warmest climates in the past 65 million years and a world-wide negative excursion of stable carbon isotopes (δ13C). To determine the location of the Paleocene-Eocene (P/E) boundary in high-latitudinal non-marine strata and to examine the magnitude of vegetation and climatic change during the warming period, the bulk carbon isotope ratios were measured in coal samples taken from several well exposed outcrops at Stenkul Fiord, Ellesmere Island, Nunavut, Canadian Arctic Archipelago. The stratigraphic sections consist of three vertical sequences (SF-P, SF-M, and P Series) that have an approximate total thickness of 74.27 m, 73.18 m, and 145 m respectively. Extending from the lower part of the P-series outcrop, three horizontal sections were taken (1, 2, and 3 Series) each spanning approximately 1 km. The bulk δ13C in the samples ranged from -23.9‰ to -28.7‰ with a background fluctuation of less than 2‰. The PETM boundary is placed in the upper portion of the P-Series between P-58 and P-60 and also in the lower portion of the SF-M and SF-P series where a sharp decrease of δ13C of up to 4.7‰ is detected. This may provide an explanation for the differing conclusions drawn from a recent palynological study and a previously published record from the same sequence. Because the C isotope measurements were based upon Metasequoia-dominated plant matter, the variation of δ13C along the vertical sequence should reflect the change of δ13C of ancient atmospheric CO2, whereas the reduced variation of δ13C in the horizontal sequences may be due to compositional differences of ancient vegetation. This study is the first isotopically marked PETM in high latitude terrestrial outcrops from the High Artic that provides a stratigraphic framework under which the mechanism of drastic climatic change and its impact on non-marine environment can be further investigated.

INTRODUCTION

The stratigraphic division differentiating the end of the Paleocene and the beginning of the Eocene divisions of the Cenozoic era is referred to as the Paleocene/Eocene boundary (P/E boundary) (Figure 1). This boundary is characterized by a brief period of negative carbon isotope excursion lasting approximately 170 thousand years, known as the Paleocene Eocene thermal maximum (PETM).[1] This event occurred approximately 55 million years ago and caused numerous disturbances in the environment, such as increased sea surface temperatures up to 5-8^{0}C, extinction of benthic foraminifera, the dispersal of plankton throughout the oceans, changes in storm patterns and their severity, and migration changes of mammals.[2,3] A prior study on the PETM concluded that in order to experience the rise in global temperatures as seen during the PETM, 5,400 to 112,000 PgC of carbon had to be released into the atmosphere and oceans.[4] This allows plants to take in more isotopically light atmospheric carbon during photosynthesis and photorespiration causing a proportional amount of stable carbon isotopes (δ^{13}C) to be stored in the tissue of the plant.

Carbon dioxide is one of the greenhouse gases driving global warming, but most climate change is caused by oscillations and abnormalities in the Earth's orbit, obliquity, tectonic plate movement, geography, greenhouse gases, and amount/distribution of solar energy.[5] These factors induce more gradual periodic changes in climate that oscillate about a mean, such as seasonal changes. The Earth's climate has changed ranging from very warm periods with ice free poles to extremely cold ice ages.[6] The changes in global climate can be reconstructed through the use of stable isotopes of carbon, hydrogen, and oxygen. In the past, δ^{18}O has been the main isotope used for the purpose of understanding past global climate trends, which may be the only means available for better predicting future global climate change.

A prior study by Sluijs et al concluded that sea surface temperatures rose from approximately 18^{0}C to over 23^{0}C during the PETM by measuring the change of δ^{13}C

in polar marine sediment samples.[7] They also noted the change in sea surface salinity tending to be more brackish during the PETM as the polar ice caps had melted creating more fresh water runoff into the ocean.[8] This study will help to fill in the gaps of previous studies that primarily use marine sedimentary or pollen data to determine the PETM by instead focusing on terrestrial sedimentary. The ancient topography of Stenkul Fiord during the PETM consisted of primarily Metasequoia forests as determined in a recent pollen study by Greenwood and Basinger.[9]

Metasequoia (Dawn Redwood) trees are C_3 plants, which are believed to be less restricting of CO_2 assimilation during photosynthesis than C_4 plants.[10] The plants take in CO_2 through stomata discriminating against the Carbon 13 isotope preferring the Carbon 12 isotope as atmospheric CO_2 levels increase.[11,12] This leads to smaller amounts of the Carbon 13 isotope being stored in the tissue of the plant producing a more negative number when calculating $\delta^{13}C$.[13]

A carbon isotopic ratio ($\delta^{13}C$) is calculated as the relative amount of Carbon 13 and the carbon 12 isotopes in comparison with a standard, as expressed in the following equation[14,15]:

$$\delta^{13}C = \left[\frac{\left({}^{13}C / {}^{12}C \right)_{spl}}{\left({}^{13}C / {}^{12}C \right)_{std}} - 1 \right] * 1000$$

SAMPLES

Samples were collected from coal bearing strata of several well exposed outcrops at Stenkul Fiord, Ellesmere Island, Nunavut, Canadian Arctic Archipelago ($77^0$20N, $83^0$26W) (Figure 2). The Eureka Sound strata at Stenkul Fiord have a total thickness of 450 meters and are composed of four members defined by Riediger.[16] This formation consists of alternating layers of mostly non-marine sandstones, mudstones, siltstones, and coal believed to be from the late Paleocene to early Eocene era based upon biostratigraphic evidence. The Stenkul Fiord Formation is faulted within the Deionian Okse Bay Group, making it difficult to determine the precise stratigraphic order and exact thickness of some strata.[17,18] The samples collected from Stenkul Fiord were form three vertical (SF-P, SF-M, and P Series) and three horizontal (1, 2, and 3 Series) stratigraphic sections at the lower part of the P Series (Figure 3).

The P Series consists of 85 samples taken from approximately 58 coal seams with an approximate total thickness of 145 m. The section is broken into two parts (northern and southern), separated by faults samples were collected from two different exposures, respectively. The southern P Series is believed to be stratigraphically higher than the section from the northern exposure making it younger in age. The northern P Series includes samples P-01 through P-60, the rest of the samples form the southern section of the P Series. Based upon previous palynological studies, it is in the upper portion of this section that the P/E boundary is expected to be located. [19] The stratigraphic gap between these two sections is immeasurable; therefore the two parts of the P Series cannot be considered a continuous section.

The SF-M and SF-P Series each contain 25 samples from 25 coal seams with an approximate total thickness of 73.18 m and 74.27 m, respectively. The SF-M Series is comparable to section 83-14 of Kalkreuth's palynological study.[20] Both these sections are believed to be stratigraphically higher than the P Series. Like the P Series, the samples forming the SF-P Series were taken from different locations.

However, the vertical distance among each location is measurable so it can be treated as one section.

The three horizontal sections extend from the lower middle portion of the northern P Series. They each span approximately 1 km with the 3 Series being stratigraphically the highest and the 1 Series the lowest. The 1 Series is comprised of 14 samples taken at equal intervals from a 1 km span of a coal seam. The 2 and 3 series are made up of 11 and 9 samples, correspondingly.

METHODS

In order to prepare samples for the elemental analyzer and isotope measurement, each sample was crushed to 0.5-1.5 mm to allow the sample to burn more uniformly and completely; thus, producing a more precise measurement for the stable isotope signals. Crushing of the samples was done at the laboratory of Department of Science and Technology at Bryant University by wrapping a small amount of each sample in tin foil and hitting it with a hammer. All these tools and the scale used in the next step were wiped clean between each measurement to prevent cross contamination of the samples.

About 6000-7000 µg of each crushed sample was measured using a micro balance (Figure 4), and placed into a 3x4 mm tin cup. Next, the tin cup was formed into a ball around the sample to allow for uniform combustion. Once weighed, the tin ball containing the sample was then placed into a well of a labeled tray in the order it was to be sent through the mass spectrometer (ThermoFinnigan Delta^{Plus} Advantage) fitted with a Costech EA at the stable isotope laboratory at the Department of Geology and Geophysics at Yale University (Figure 5).

The mass spectrometer measured the amount of carbon in each sample by first bombarding the sample with high energy electrons. The electron beam ionizes the atoms of each element contained in the sample. The positively charged ions are then accelerated to the same velocity into a uniform magnetic field, where their trajectory (F) changes according to:

$$F = vqB = \frac{mv^2}{r}$$

$$\therefore m = \frac{rqB}{v}$$

Where r = radius of curvature, m = mass of particle, v = particle velocity, q = elementary charge, and B = magnetic flux.[21] The trajectory of each particle is therefore a function of its mass. The accelerated particles are sent through a tube of a given radius, so that only ions of a certain mass will reach the designated collector.

[22] Since m is a function of B, the intensity, or number of particles collected per unit time, is plotted against the magnetic flux resulting in a series of peaks (Figure 6), each of which corresponds to a certain element such as $\delta^{13}C$. [23]

Every tenth sample measured was run through the elemental analyzer three times in order to test the accuracy and precision of the machine. The average standard deviation of these samples was .127 per mil. Also, 4000 µg of cocoa standards containing -28.41‰ $\delta^{13}C$ and 5.24‰ ^{15}N were measured by the elemental analyzer between every eleven samples. In addition, a series of cocoa samples measured ranging from 1000 µg to 6000 µg were placed as the first and last three samples of a run for each measurement to test the stability of the machine. The elemental analyzer connected to a mass spectrometer measures the percentage of C and N as well as $\delta^{13}C$ and ^{15}N stable isotopic ratios and tabulated in a spreadsheet file as input (Tables 1-7).

The spreadsheet file was then filtered keeping only the data from the third and fourth, or carbon and nitrogen peaks. From there the C/N ratio was calculated by dividing % N into % C. The $\delta^{13}C$ ratio was then corrected by adding the difference of the average $\delta^{13}C$ and the known amount of $\delta^{13}C$ in the cocoa samples. Another correction was applied to $\delta^{13}C$ in order to account for the continuous light the plants in the Canadian High Artic would have received. To do this 1.93‰ was added to the value of $\delta^{13}C$ since plants in continuous light have on average a 1.93‰ more negative $\delta^{13}C$ than plants not receiving continuous light (Hong Yang unpublished data). In order to correct $\delta^{15}N$ a more complex equation was applied using the amplitude, order the sample was ran, and known amount of $\delta^{15}N$ in cocoa. The N data are not used in this study as N isotope bears no association P/E boundary.

RESULTS

We are particularly interested in profound negative carbon isotopic changes. The most dramatic decrease of negative $\delta^{13}C$ values can be seen in the upper portion of the Northern P Series between samples P-58 and P-60 (Figure 7). Here the $\delta^{13}C$ decreased to -28.4‰ from the mean value of -25.43‰. After correcting the data for the continuous light plants receive in the high artic by adding 1.93‰, it really decreased to -26.5‰ from the mean value of -23.5‰. The rest of the samples in this section show $\delta^{13}C$ fluctuations around the corrected mean of -23.5‰ varying in either direction of up to 1‰. The Southern P Series results also show $\delta^{13}C$ fluctuating between -22.5‰ and -24.5‰ consistent with the background fluctuation of the Northern P Series.

Another large negative excursion is seen at the bottom of the vertical SF-M section. Like the Northern P Series, the $\delta^{13}C$ decreased to -26.8‰ in sample SF-M-02 (Figure 7). There is also another smaller peak of negative $\delta^{13}C$ excursion between SM-F-11 through SM-F-14 of -25.1‰. The rest of the samples in the sequence show $\delta^{13}C$ oscillating between -22.5‰ and -24‰. In conjunction with the SF-M Series, the SF-P Series also produced a large negative $\delta^{13}C$ excursion in the lower part of the vertical sequence, and for the most part the same background fluctuations (Figure 7).

The three horizontal sections show minimal changes in the $\delta^{13}C$. The $\delta^{13}C$ in the 1 Series varied between -22.5‰ and -24.5‰, while the 2 Series and 3 Series varied between -22‰ and

-24‰ and -23‰ and -25‰, respectively (Figure 9).

DISCUSSION

The results from the vertical sections should reveal how atmospheric CO_2 and global temperatures changed over time. As $\delta^{13}C$ values decreased in the upper portion of the northern P Series and the lower portions of the SF-M and SF-P Series, the ancient atmospheric CO_2 and global temperatures increased indicating the possible placement for P/E boundary. These results support one of the hypotheses of this study, which stated that the PETM occurred in upper portion of the northern P Series.[24] However, they also support the differing viewpoint of previous studies placing the boundary in the lower portions of the SF-M and SF-P Series. They conflict because the original perception of how the sections stratigraphically relate to each other placed the SF-M and SF-P series above the southern exposure of the P Series, which was above the northern exposure of the P Series (Figure 3). This means that the results would support the P/E boundary occurring twice, once in the older P series and again in the younger time period of the SF-M and SF-P series. Since there has only been one P/E boundary a theory aligning these findings must be discussed.

The SF-M and SF-P Series are stratigraphically higher than the P Series, but the vertical distance between them is unknown due to the unconformities in the Stenkul Fiord area. This leaves the possibility for overlapping of the sections open for discussion. Our results show peaks of negative $\delta^{13}C$ excursion in the top of the northern P Series and at the bottom of both the SF-M and SF-P Series. We may therefore speculate that these peaks are in fact from the same time period and the graphs of the P and SF-M Series may overlap by two samples to form a continuous section. To be more specific, the sample P-60 and SF-M-02 may be from the same coal bearing stratum, making it the tentative location of the P/E boundary (Figures 7, 8). This new perception of how the sampled sections stratigraphic relate to each other would reconcile the two competing theories.

The PETM is characterized by the rapid increase of global surface temperatures. Pagani's study on artic hydrology suggests a far larger scale of both bulk and

molecular C isotope excursion occurring abruptly within a more gradual isotopic gradient change.[25] It is possible that the absolute maximum change in the carbon isotope gradient was missed in this study due to the low sampling density of the vertical stratigraphic sections. Samples were only taken from coal bearing strata with no fixed distance between samples. The sampling in this study also became less dense in the stratum of interest than other strata in the sequence due to the limitation of stratigraphic lithology (Figure 7).

As seen in the results, the horizontal sections have much less variation of $\delta^{13}C$ than the vertical sections (Figure 9). This can be expected because each horizontal section is from one stratum, which implies all the samples are from the same time period. The amount of CO_2 and its carbon isotopic value found in the ancient atmosphere of each horizontal section is then assumed to be fixed. The little variation that is seen in the $\delta^{13}C$ can be explained by the variation of the ancient vegetation across the distance sampled.

CONCLUSIONS

By measuring the $\delta^{13}C$ in terrestrial sediments from the Canadian High Artic, we have detected large negative $\delta^{13}C$ excursions in the upper portion of the P Series from the northern exposure and in the bottom both the SF-M and SF-P Series. The results showed a discrepancy in the location of the P/E boundary because the large negative $\delta^{13}C$ excursion in the upper portion of the P Series from the northern exposure and in both SF-M and SF-P Series indicate the location of the PETM in two different time periods. This discrepancy can be resolved by shifting the view of how the sampled sections stratigraphically relate to one another. The original relationship had the SF-M and SF-P Series above the P Series from the southern exposure, which was then above the P Series from the northern exposure (Figure 3). The proposed view on the stratigraphic relationship of the samples keeps the SF-M and SF-P stratigraphically at the top, or younger than the other series, but allows for the P Series to overlap (Figure 8). The P Series from the northern exposure remains stratigraphically above the series from the northern exposure, but now is stratigraphically equivalent to the middle of the S-FM and S-FP Series. The top portion of the P Series from the northern exposure would now be considered stratigraphically equivalent to the bottom of the S-FM and S-FP Series. This aligns the large peaks of $\delta^{13}C$ creating one agreed upon location of the P/E boundary.

FURTHER WORK

Now that a more specific location of the maximum change in ancient carbon isotopes has been established, further studies may more densely sample the location to more accurately pinpoint the maximum change in negative $\delta^{13}C$ excursion indicating the PETM. This may be difficult on these sections since coal seams are also less frequent in the strata where the P/E boundary is believed to be located. Further pollen studies that more densely sample the strata may help to fill in the gaps and determine the height of the PETM. If possible, it may also be helpful to better examine how these sections stratigraphically relate to one another.

ACKNOWLEDGMENTS

I would like to especially thank Drs. Hong Yang, Brian Blais, Ben LePage, and Mark Pagani for all their time, input, and guidance throughout this project. I would also like to thank Hong and Ben for providing the samples and the opportunity to work on this project. Dr. Gerry Olack is thanked for teaching me how to use all the lab equipment and answering my many questions. A special thank you goes to NASA RI Space Grant Consortium for the funding necessary to conduct this study. I also thank the Bryant University Honors Program and the Department of Science and Technology for the additional funding to present these results at Sigma Xi conference. More specifically, I thank Dr. Ken Sousa for running the honors program and his continuous encouragement and support.

APPENDICES

Figure 1.

Geological Timeline
(modified from Tarbuck and Lutgens (2006) Earth Science, 11th Edition, Pearson-Prentice Hall)

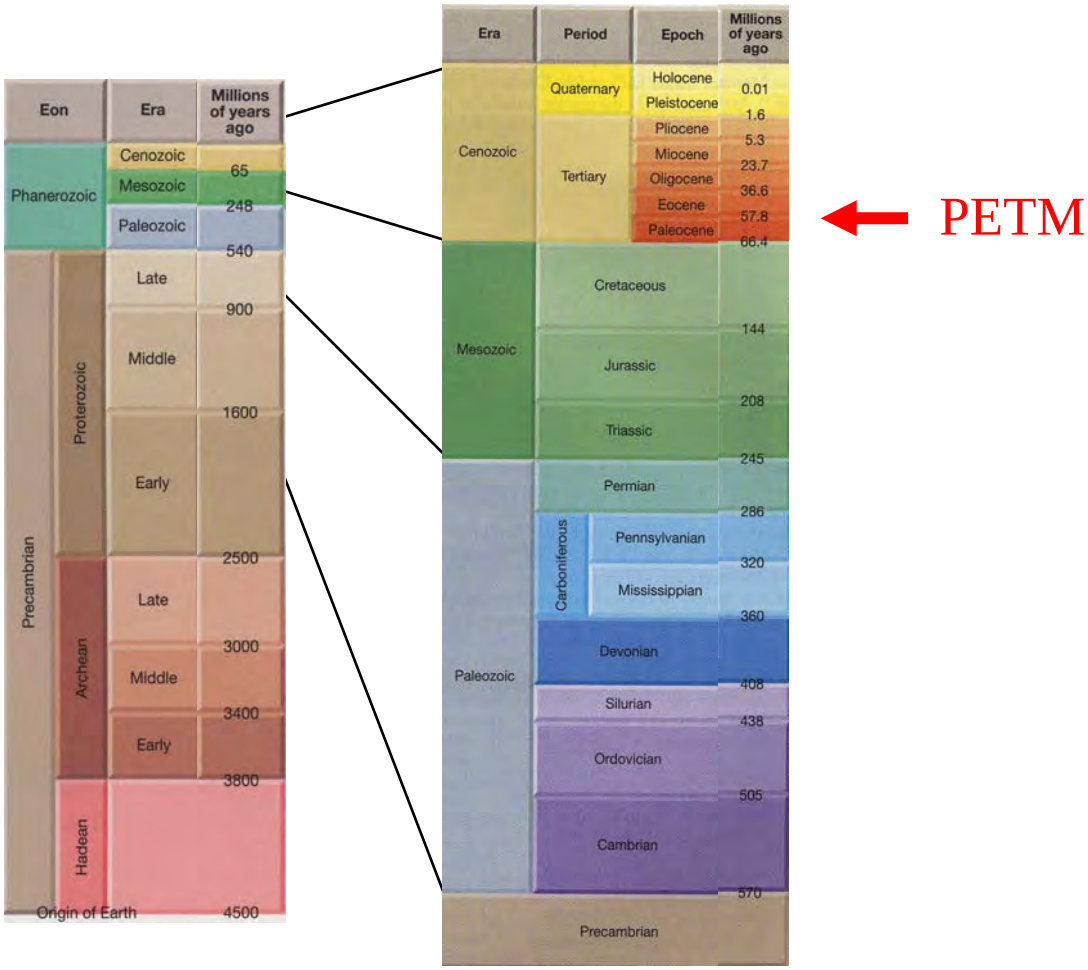

Figure 2.

Map of Canadian High Artic
(From Hong Yang et. al. Biomolecular preservation of Tertiary Metasequoia Fossil Lagerstatten revealed by comparative pyrolysis analysis. Rev. Paleobot. Pal. 134. 237-256 (2004))

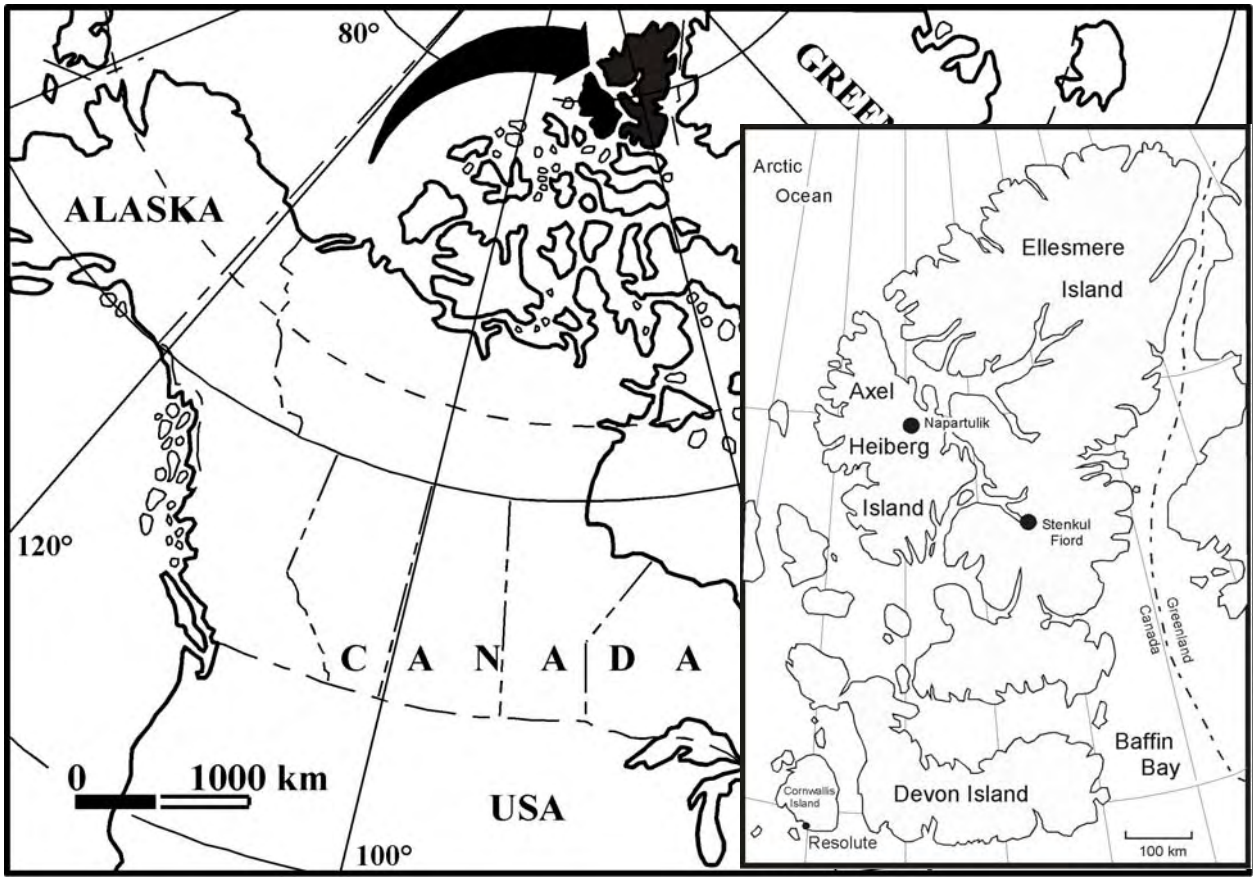

This is a map of the Canadian High Artic with a more detailed map of Ellesmere Island marking the location the samples were taken from with a black dot.

Figure 3.

Original View of Sections and Possible Locations of the P/E Boundary

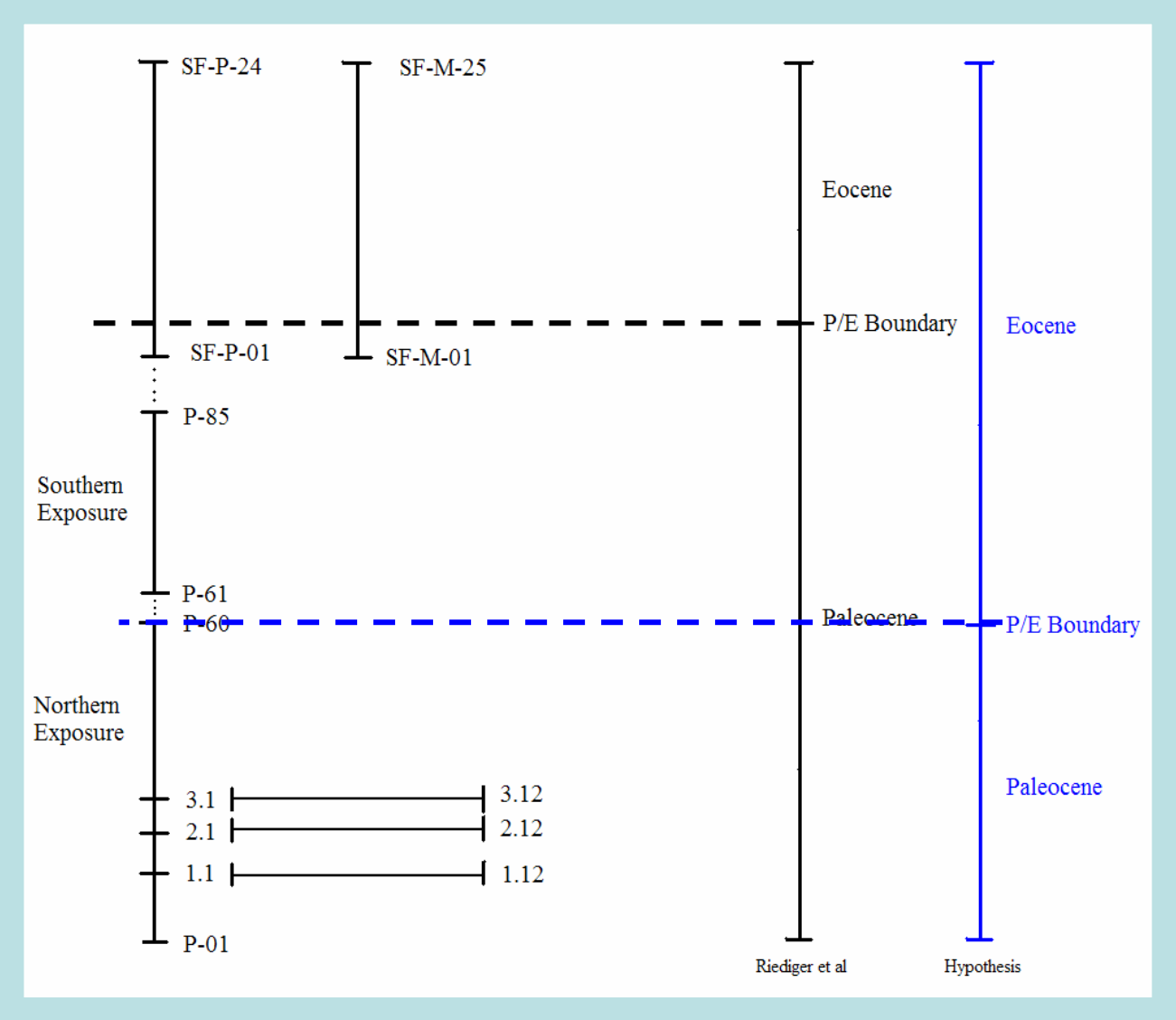

The top of this diagram is stratigraphically higher or closer to the surface of the Earth making samples toward the top younger than the samples below them. The original perception had the SF-M and SF-P Series stratigraphically higher than the P Series with no overlapping. The black dotted line represents the believed location of the PETM by Reidiger et al and the blue dotted line represents the believed location of the PETM going into this study.

Figure 4.

Micro Balance

Figure 5.

ThermoFinnigan Delta^{Plus} Advantage fitted with a Costech EA

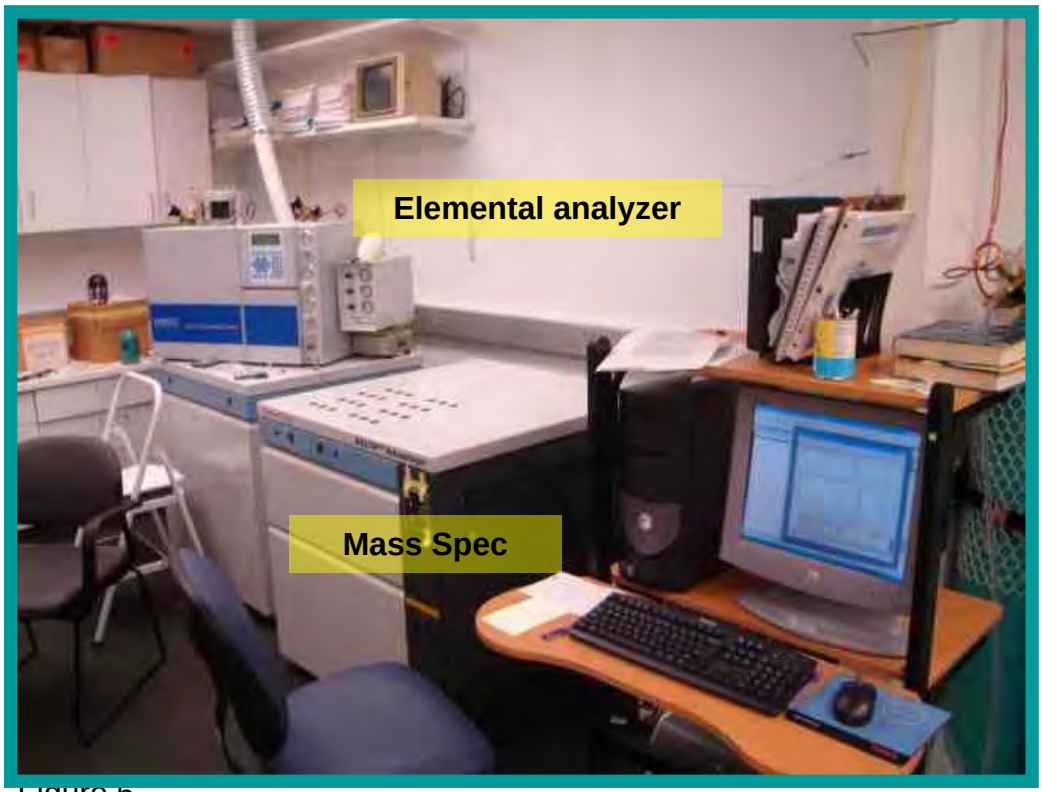

Figure 6.

Example of Carbon Intensity for One Sample

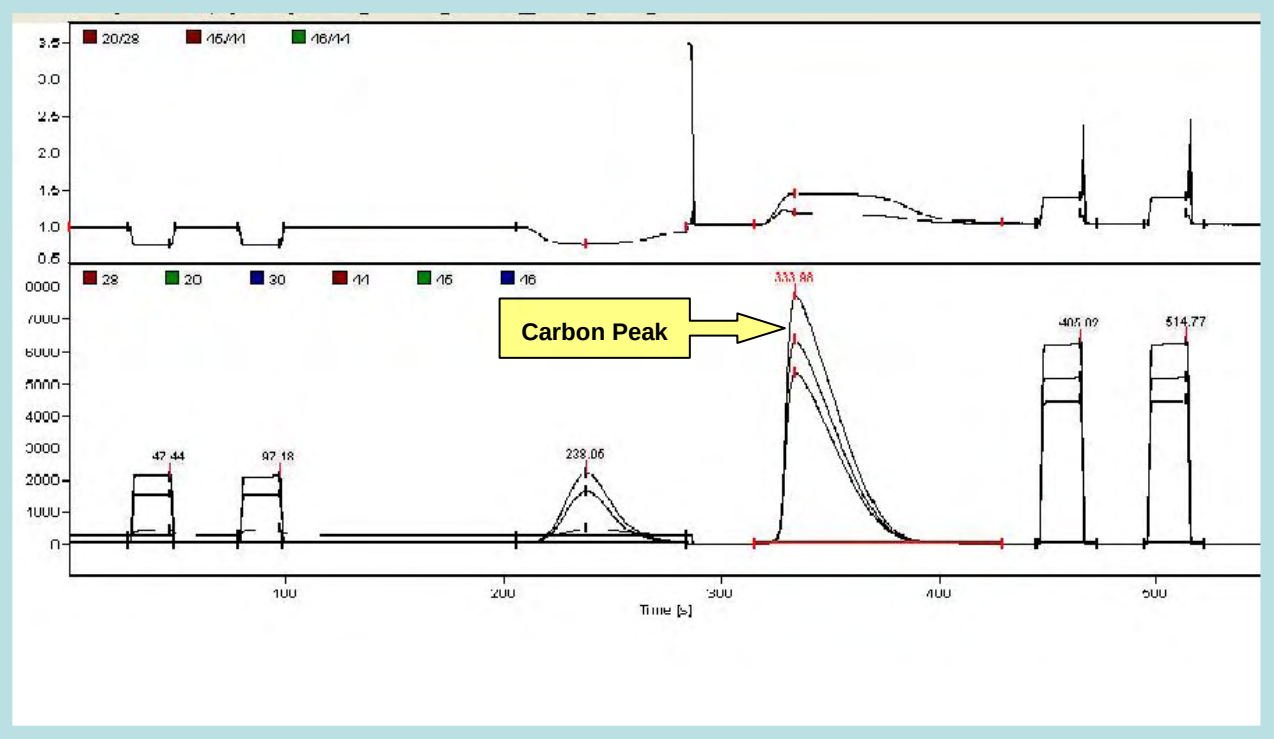

The peaks show the intensity, or amount, of each element in the sample. The third peak represents the intensity of the nitrogen 15 isotope, and the fourth peak represents the intensity of the carbon 13 isotope.

Figure 7.

Results of Vertical Sections

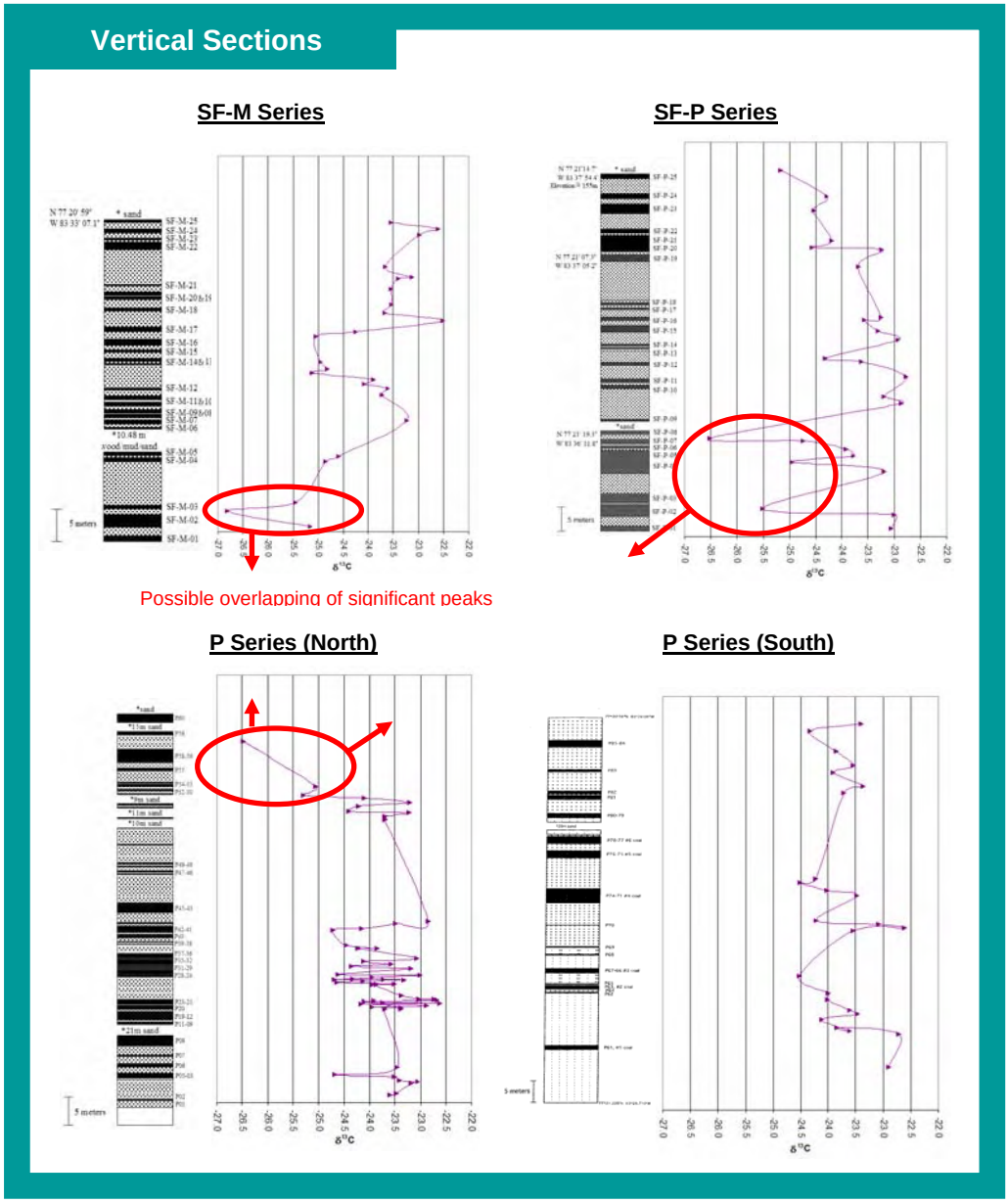

This figure shows a scaled stratigraphic diagram of each section next to a graph of the ^{13}C contained in each sample of the section. The stratigraphic diagrams portray coal seams in solid black whereas sand, mudstone, and wood are portrayed by the other patterns. The sample number is indicated to the right of the coal seam it came from. The significant negative peaks of the corrected ^{13}C are circled in red and the arrows point out how the top two graphs may overlap with the bottom left graph. The bottom right graph is now proposed to overlap the middle part of both graphs on the top.

Figure 8.

Proposed View of Section

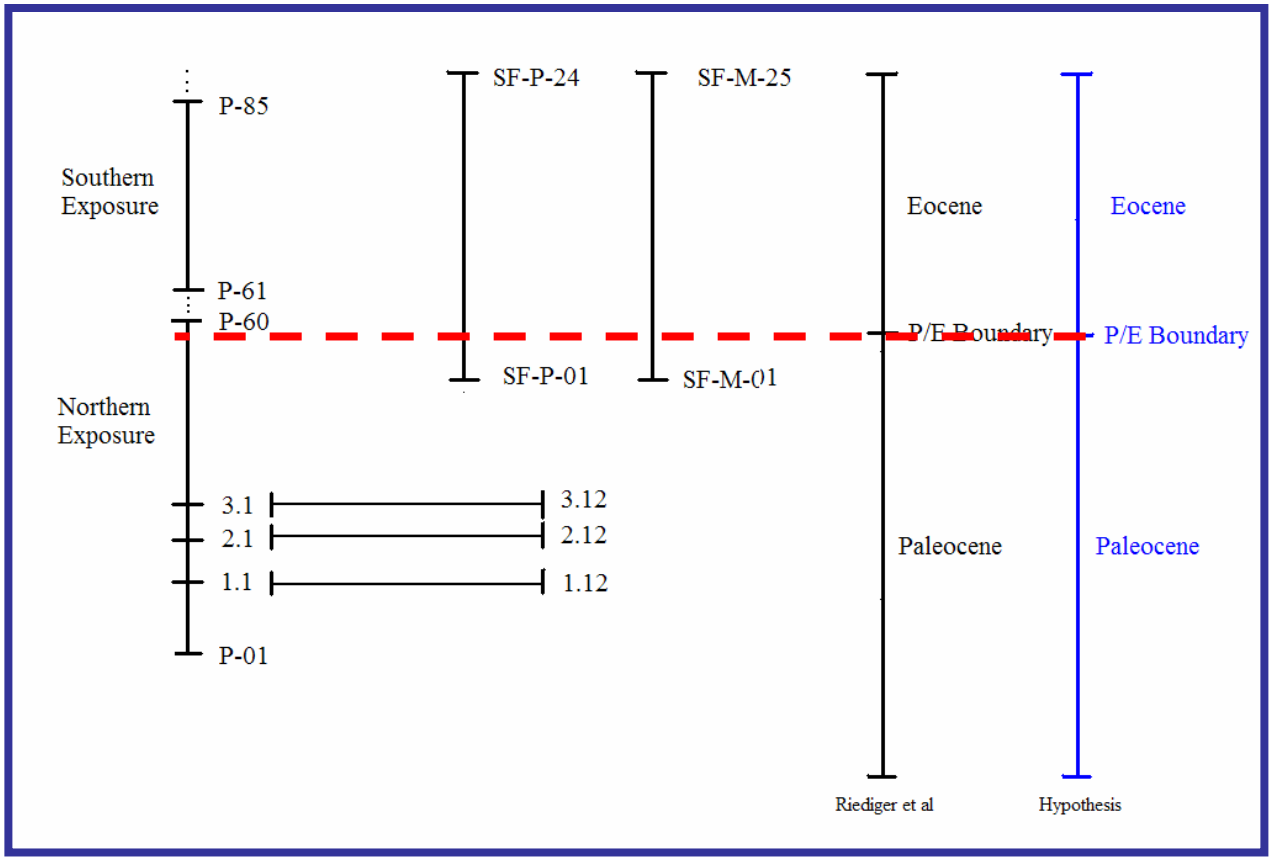

After viewing the results from this study, a reorganization of how the sections relate to one another stratigraphically is introduced to align the believed locations of the P/E boundary. This can be done since the exact relationship of the sections remains unknown due to unconformities in the sample site. The reorganization involves overlapping the top portion of the P Series with the bottom portions of the SF-M and SF-P Series. The new believed location of the PETM is marked by the red dotted line.

Figure 9.

Results of Horizontal Sections

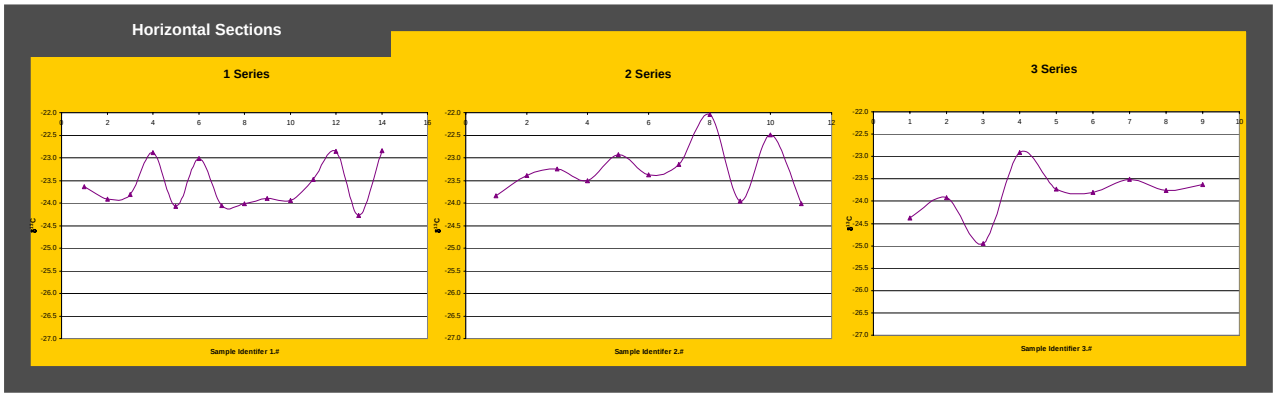

The horizontal sections show much less variation than the vertical sections as seen in the graphs above relating the corrected amount of ^{13}C to the sample number since the samples were taken at equal intervals.

Data

- Highlighted data represents an average data from three runs of the same sample

Table 1

Identifier	Amount	Amt %C	Amt%N	^{13}C	^{15}N	C/N Ratio	Corrected ^{13}C
P Series (South)							
P-85	6881	18.47	0.61	-25.33	2.08	30.19	-23.40
P-84	6653	14.74	0.52	-26.26	2.05	28.07	-24.33
P-83	6966	42.09	1.10	-25.79	2.62	38.15	-23.86
P-82	6194	45.63	1.26	-25.47	2.79	36.33	-23.54
P-81	7040	23.72	0.76	-25.84	2.59	31.36	-23.91
P-80	6955	19.90	0.64	-25.30	2.18	31.02	-23.37
P-79	6738	21.02	0.65	-25.64	2.65	32.26	-23.71
P-78	6597	15.02	0.54	-26.16	2.28	27.98	-24.23
P-77	6985	32.63	1.03	-26.45	2.37	31.64	-24.52
P-76	6438	18.53	0.66	-25.96	2.16	27.99	-24.03
P-75	6391	21.69	0.80	-25.41	2.65	27.13	-23.48
P-74	6798	25.69	0.82	-26.14	2.76	31.36	-24.21
P-73	7028	28.03	0.94	-25.01	2.79	29.84	-23.08
P-72	6237	19.34	0.69	-24.54	2.40	27.95	-22.61
P-71	7023	17.22	0.64	-25.47	2.33	27.01	-23.54
P-70-2001	6620	10.31	0.44	-26.45	1.95	23.69	-24.52
P-69	6637	48.99	1.47	-25.93	2.80	33.34	-24.00
P-68	6820	9.44	0.41	-25.94	1.97	22.98	-24.01

P-67	6403	19.97	0.77	-25.54	2.65	25.98	-23.61
P-66	6845	59.63	1.57	-25.39	2.89	37.95	-23.46
P-65	6276.33	29.34	0.86	-26.05	2.94	33.98	-24.12
P-64	6501	10.38	0.43	-25.54	2.38	23.92	-23.61
P-63	6982	12.90	0.50	-25.78	2.66	26.00	-23.85
P-62	6577	14.70	0.54	-24.65	2.29	27.10	-22.72
P-61	6930	58.84	1.42	-24.84	2.42	41.51	-22.91

Table 2

Identifier	Amount	Amt %C	Amt%N	^{13}C	^{15}N	C/N Ratio	Corrected ^{13}C
P Series (North)							
P-60	6260	18.87	0.58	-28.40	2.12	32.53	-26.47
P-59	6355	31.42	0.83	-26.99	2.50	37.71	-25.06
P-58	6730	13.95	0.49	-27.23	2.65	28.49	-25.30
P-57	6107	24.72	0.78	-26.04	3.19	31.89	-24.11
P-56	6842	15.18	0.50	-25.14	3.05	30.27	-23.21
P-55	6477.67	12.27	0.46	-26.15	2.16	26.74	-24.22
P-54	6810	11.60	0.46	-26.33	1.89	25.47	-24.40
P-53	6419	16.25	0.52	-25.16	2.69	31.06	-23.23
P-52	6723	14.25	0.44	-25.64	1.56	32.05	-23.71
P-51	6905	8.03	0.30	-25.64	1.49	26.78	-23.71
P-50	6457.00	8.25	0.31	-25.64	1.72	26.81	-23.71
P-49-2001	6586	53.40	1.00	-24.79	3.43	53.62	-22.86
P-48-2001	6285	17.51	0.62	-25.43	2.08	28.26	-23.50
P-47-2001	6746	28.71	0.94	-26.10	2.42	30.55	-24.17
P-46-2001	6737	25.12	0.86	-26.65	2.07	29.28	-24.72
P-45-2001	6064	11.35	0.43	-26.39	1.73	26.52	-24.46
P-44-2001	6015	56.97	1.57	-25.78	1.68	36.20	-23.85
P-43-2001	6403	40.93	1.26	-26.16	2.63	32.43	-24.23
P-42-2001	6641	40.86	1.14	-25.01	2.31	35.80	-23.08
P-41-2001	6181	19.61	0.67	-26.05	1.84	29.33	-24.12
P-40-2001	6445.33	26.85	0.86	-25.51	2.22	31.12	-23.58
P-39-2001	6678	13.92	0.57	-26.29	2.06	24.63	-24.36
P-38-2001	6546	38.47	1.11	-25.12	2.30	34.64	-23.19
P-37-2001	6920	25.36	0.80	-26.55	1.84	31.58	-24.62
P-36-2001	6978	40.15	1.23	-24.94	2.56	32.77	-23.01
P-35-2001	6924	21.42	0.76	-25.89	1.88	28.08	-23.96
P-34-2001	6275	9.50	0.41	-26.27	2.04	23.26	-24.34
P-33-2001	6789	26.62	0.89	-26.62	2.07	29.86	-24.69
P-32-2001	6982	17.89	0.63	-25.66	2.39	28.34	-23.73
P-31-2001	6634	17.89	0.65	-25.26	1.88	27.40	-23.33
P-30-2001	6364.33	22.50	0.80	-26.07	1.84	28.25	-24.14
P-29-2001	6384	29.28	0.98	-26.58	1.85	29.82	-24.65
P-28-2001	6740	18.13	0.65	-25.45	2.01	27.80	-23.52

P-27-2001	5997	14.21	0.53	-25.80	1.52	26.98	-23.87
P-25-2001	6595	14.00	0.53	-25.87	1.42	26.27	-23.94
P-24-2001	6336	16.34	0.26	-6.66	1.45	63.75	-4.73
P-23-2001	6587	25.34	0.87	-25.31	2.09	29.28	-23.38
P-22-2001	6423	16.16	0.57	-24.97	2.42	28.59	-23.04
P-21-2001	6963	34.70	1.05	-24.67	2.74	32.91	-22.74
P-20-2001	6657.00	21.79	0.79	-24.61	2.81	27.73	-22.68
P-19-2001	6832	30.67	0.96	-25.84	2.68	32.04	-23.91
P-18-2001	6544	19.14	0.66	-26.04	2.34	29.19	-24.11
P-17-2001	6003	32.03	1.05	-25.66	2.46	30.52	-23.73
P-16-2001	6736	11.39	0.42	-24.55	2.24	27.31	-22.62
P-15-2001	6890	25.78	0.84	-26.11	2.12	30.74	-24.18
P-14-2001	6814	20.57	0.68	-24.81	2.47	30.44	-22.88
P-13-2001	6635	26.74	0.89	-25.87	2.21	29.94	-23.94
P-12-2001	6220	32.65	1.04	-25.32	2.80	31.53	-23.39
P-11-2001	6959	5.89	0.31	-25.32	2.06	19.23	-23.39
P-10-2001	6662.67	45.92	1.30	-25.32	2.46	35.34	-23.39
P-09-2001	6680	3.14	0.24	-25.64	0.77	13.10	-23.71
P-08-2001	6740	33.09	1.14	-25.39	2.25	29.13	-23.46
P-07-2001	6601	49.76	1.38	-26.61	1.55	36.04	-24.68
P-06-2001	6960	28.41	0.96	-25.46	2.53	29.67	-23.53
P-05-2001	6834	29.51	1.02	-25.34	2.24	28.89	-23.41
P-04-2001	6686	22.15	0.87	-24.99	2.55	25.32	-23.06
P-03-2001	6184	53.82	1.45	-25.12	2.85	37.13	-23.19
P-02-2001	6471	56.67	1.73	-25.41	2.02	32.85	-23.48
P-01-2001	6354.50	54.53	1.78	-25.53	2.18	30.60	-23.60

Table 3

Identifier	Amount	Amt %C	Amt%N	^{13}C	^{15}N	C/N Ratio	Corrected ^{13}C
SF-M Series							
SF-M-01	6932	54.39	1.32	-27.08	3.11	41.21	-25.15
SF-M-02	6253	46.44	1.31	-28.74	2.30	35.45	-26.81
SF-M-03	6980	35.64	0.87	-27.39	2.88	41.19	-25.46
SF-M-04	6726	55.59	1.51	-26.78	2.70	36.71	-24.85
SF-M-05	6741	41.33	0.73	-26.52	2.91	56.24	-24.59
SF-M-06	6453	35.66	0.96	-25.16	2.95	37.22	-23.23
SF-M-07	6239	44.35	1.20	-25.66	2.80	36.91	-23.73
SF-M-08	6959	52.32	1.28	-25.54	2.63	40.73	-23.61
SF-M-09	6380	50.70	1.24	-26.01	3.31	40.80	-24.08
SF-M-10	6085.00	44.50	0.98	-25.83	3.03	45.51	-23.90
SF-M-11	6786	37.06	0.94	-27.05	2.27	39.30	-25.12
SF-M-12	6630	44.02	0.97	-26.74	2.88	45.31	-24.81
SF-M-13	6749	15.24	0.45	-26.89	2.60	33.85	-24.96
SF-M-14	6352	21.56	0.61	-26.98	2.56	35.40	-25.05

SF-M-15	6492	39.87	1.00	-26.18	2.44	39.78	-24.25
SF-M-16	6896	11.38	0.38	-24.44	2.42	30.30	-22.51
SF-M-17	6500	43.91	1.04	-25.60	2.76	42.13	-23.67
SF-M-18	6860	55.08	1.35	-25.46	2.73	40.67	-23.53
SF-M-19	6579	52.27	1.12	-25.48	2.90	46.68	-23.55
SF-M-20	6788.33	37.90	0.95	-25.33	3.05	39.95	-23.40
SF-M-21	6021	30.68	0.79	-25.06	2.87	38.84	-23.13
SF-M-22	6582	33.66	0.81	-25.59	2.50	41.67	-23.66
SF-M-23	6742	42.55	0.98	-24.91	2.71	43.27	-22.98
SF-M-24	6781	30.07	0.74	-24.54	2.27	40.77	-22.61
SF-M-25	6038	47.26	1.13	-25.47	3.54	41.96	-23.54

Table 4

Identifier	Amount	Amt %C	Amt%N	^{13}C	^{15}N	C/N Ratio	Corrected ^{13}C
SF-P Series							
SF-P-01	6436	32.46	0.69	-25.00	2.24	46.73	-23.07
SF-P-02	6912	19.90	0.74	-24.93	4.18	27.04	-23.00
SF-P-03	6343	42.79	0.94	-27.44	3.16	45.62	-25.51
SF-P-04	6560	41.10	0.95	-25.12	4.54	43.36	-23.19
SF-P-05	6727	42.56	1.09	-26.89	6.60	39.10	-24.96
SF-P-06	6524	28.72	0.74	-25.71	3.98	38.81	-23.78
SF-P-07	6397	24.82	0.64	-25.86	3.15	38.78	-23.93
SF-P-08	6018	52.96	1.20	-26.66	7.70	44.04	-24.73
SF-P-09	6784	40.85	0.95	-28.44	8.57	42.95	-26.51
SF-P-10	6525.67	40.62	0.85	-24.80	4.02	48.03	-22.87
SF-P-11	6591	51.35	1.03	-25.12	9.20	49.65	-23.19
SF-P-12	6688	38.23	0.83	-24.70	2.73	45.88	-22.77
SF-P-13	6383	28.53	0.63	-25.55	1.31	45.21	-23.62
SF-P-14	6870	21.64	0.57	-26.24	1.03	38.26	-24.31
SF-P-15	6375	35.59	0.84	-24.85	2.23	42.28	-22.92
SF-P-16	6991	16.91	0.46	-25.25	-0.16	36.52	-23.32
SF-P-17	6643	45.49	1.02	-25.50	9.43	44.52	-23.57
SF-P-18	6336	37.95	0.83	-25.19	2.25	45.48	-23.26
SF-P-19	6311	57.73	1.11	-25.62	1.64	52.20	-23.69
SF-P-20	6625.33	32.37	0.73	-25.18	0.30	44.50	-23.25
SF-P-21	6189	31.11	0.77	-26.50	-0.27	40.30	-24.57
SF-P-22	6815	44.76	1.00	-26.12	10.14	44.98	-24.19
SF-P-23	6050	20.89	0.55	-26.47	-2.36	37.79	-24.54
SF-P-24	6886	41.17	1.01	-26.22	8.27	40.60	-24.29
SF-P-25	6312	54.56	1.29	-27.10	9.30	42.28	-25.17

Table 5

Identifier	Amount	Amt %C	Amt%N	^{13}C	^{15}N	C/N Ratio	Corrected ^{13}C
1 Series							
1.1	6184	17.63	0.64	-25.56	2.26	27.71	-23.63
1.2	6692	21.03	0.73	-25.85	2.60	28.73	-23.92
1.3	6545	16.74	0.60	-25.74	2.44	27.70	-23.81
1.4	6877	30.41	0.99	-24.81	2.58	30.61	-22.88
1.5	6816	16.87	0.61	-26.00	2.33	27.71	-24.07
1.6	6823	26.06	0.87	-24.94	2.50	29.83	-23.01
1.7	6273	20.79	0.73	-25.99	2.50	28.68	-24.06
1.8	6800	24.84	0.83	-25.94	2.80	29.78	-24.01
1.9	6677	24.38	0.78	-25.82	2.45	31.12	-23.89
1.10	6731.67	18.68	0.68	-25.87	2.63	27.28	-23.94
1.11	6925	21.12	0.76	-25.41	2.45	27.84	-23.48
1.12	6334	13.66	0.51	-24.78	2.74	27.05	-22.85
1.13	6437	22.72	0.78	-26.21	2.33	29.07	-24.28
1.14	6797	11.45	0.45	-24.78	2.72	25.59	-22.85

Table 6

Identifier	Amount	Amt %C	Amt%N	^{13}C	^{15}N	C/N Ratio	Corrected ^{13}C
2 Series							
2.1	6091	20.81	0.77	-25.76	2.31	27.00	-23.83
2.2	6452	24.02	0.84	-25.32	2.59	28.48	-23.39
2.3	6981	17.68	0.64	-25.17	2.19	27.80	-23.24
2.4	6551.00	29.93	0.82	-25.43	2.63	36.66	-23.50
2.5	6342	23.83	0.88	-24.86	2.38	26.92	-22.93
2.6	6128	27.45	0.96	-25.31	2.62	28.60	-23.38
2.7	6030	25.68	0.88	-25.07	2.45	29.29	-23.14
2.8	6383	17.50	0.62	-23.98	2.56	28.26	-22.05
2.9	6389	29.63	1.00	-25.89	2.44	29.50	-23.96
2.1	6278	18.63	0.72	-24.42	2.29	25.80	-22.49
2.11	6695	23.30	0.74	-25.95	2.09	31.54	-24.02

Table 7

Identifier	Amount	Amt %C	Amt%N	^{13}C	^{15}N	C/N Ratio	Corrected ^{13}C
3 Series						#DIV/0!	
3.1	6875	28.36	0.91	-26.30	3.10	31.25	-24.37
3.2	6816	30.38	0.99	-25.86	2.85	30.72	-23.93
3.3	6432	26.44	0.89	-26.87	2.30	29.70	-24.94
3.4	6256	25.10	0.90	-24.85	2.57	27.77	-22.92
3.5	6443.67	21.06	0.70	-25.66	2.71	30.01	-23.73
3.6	6337	26.94	0.85	-25.73	2.84	31.51	-23.80
3.7	6981	21.43	0.70	-25.44	2.70	30.42	-23.51
3.8	6301	38.84	1.25	-25.68	3.36	31.00	-23.75
3.9	6655	23.37	0.76	-25.56	2.64	30.94	-23.63

REFERENCES

[11] Pagani, Mark et al. An Ancient Carbon Mystery. Science 314. 1556-1557 (2006)
[2] Zachos, James et al. A transient rise in tropical sea surface temperature during the Paleocene-Eocene thermal maximum.Science 302. 1551-1554 (2003)
[3] Sluijs, Appy et al. Subtropical Artic Ocean temperatures during the Paleocene/Eocene thermal maximum. Nature 441. 610-613 (2006)
[4] Pagani, Mark et al. An ancient carbon mystery. Science 304. 1556-1557 (2006)
[5] Zachos, James et al. Trends, Rhythms, and Abberations in Global Climate 65 Ma to Present. Science 292. 686-692 (2001)
[6] Zachos, James et al. Trends, Rhythms, and Abberations in Global Climate 65 Ma to Present. Science 292. 686-692 (2001)
[7] Sluijs, Appy et al. Subtropical Artic Ocean temperatures during the Paleocene/Eocene thermal maximum. Nature 441, 610-613 (2006)
[8] Sluijs, Appy et al. Subtropical Artic Ocean temperatures during the Paleocene/Eocene thermal maximum. Nature 441, 610-613 (2006)
[9] Greenwood, David R. and Basinger, James F. The paleoecology of high-latitude Eocene swamp forests from Axel Heiberg Island, Canadian High Artic. Review of Paleobotany and Palynology 81. 83-97 (1994)
[10]Farquhar, Graham D. and Sharkey, Thomas D. Stomatal Conductance and Photosynthesis. Annu. Rev. Plant Physiol. 33. 317-345. (1982)
[11] Farquhar, Graham D. et al. Models of Photosynthesis. Plant Physiology 125. 42-45. (2001)
[12] White, W. M. Geochemistry. CH 9 Stable Isotope Geochemistry.358-414 (2005)
[13] White, W. M. Geochemistry. CH 9 Stable Isotope Geochemistry.358-414 (2005)
[14] Faure, Gunther. Principles of Isotope Geology. 2nd ed. New York. John Wiley and Sons. p 495. 1986
[15] Faure, Gunther. Principles of Isotope Geology. 2nd ed. New York. John Wiley and Sons. p 495. 1986
[16] Kalkreuth, W.D. et al. Petrological, Palynological and geochemical characteristics of Eureka Sound Group coals (Stenkul Fiord, southern Ellesmere Island, Artic Canada). Int. Journal of Coal Geology 30. 151-182 (1996)
[17] Kalkreuth, W.D. et al. Petrological, Palynological and geochemical characteristics of Eureka Sound Group coals (Stenkul Fiord, southern Ellesmere Island, Artic Canada). Int. Journal of Coal Geology 30. 151-182 (1996)
[18] Riediger, C.L. and Bustin R.M. The Eureka Sound formation, Ellesmere Island. Bull. Can. Pet. Geol. 35(2), 123-142 (1987)
[19] Kalkreuth, W.D. et al. Petrological, Palynological and geochemical characteristics of Eureka Sound Group coals (Stenkul Fiord, southern Ellesmere Island, Artic Canada). Int. Journal of Coal Geology 30. 151-182 (1996)
[20] Kalkreuth, W.D. et al. Petrological, Palynological and geochemical characteristics of Eureka Sound Group coals (Stenkul Fiord, southern Ellesmere Island, Artic Canada). Int. Journal of Coal Geology 30. 151-182 (1996)
[21] Faure, Gunther. Principles of Isotope Geology. 2nd ed. New York. John Wiley and Sons. p 495. 1986
[22] Faure, Gunther. Principles of Isotope Geology. 2nd ed. New York. John Wiley and Sons. p 495. 1986
[23] Faure, Gunther. Principles of Isotope Geology. 2nd ed. New York. John Wiley and Sons. p 495. 1986
[24] Riediger, C.L. and Bustin R.M. The Eureka Sound formation, Ellesmere Island. Bull. Can. Pet. Geol. 35(2), 123-142 (1987)
[25] Pagani, Mark et al. Artic hydrology during global warming at the Paleocen/Eocene thermal maximum. Nature 422, 671-674 (2006)